Bimetallic Pd–Cu Catalysts: X-Ray Diffraction and Theoretical Modeling Studies

Ling Zhu,* K. S. Liang,† B. Zhang,† J. S. Bradley,†‡ and Andrew. E. DePristo*,§

*Ames Laboratory, U.S. Department of Energy, and §Department of Chemistry, Iowa State University, Ames, Iowa 50011; †Corporate Research, Exxon Research and Engineering Company, Annandale, New Jersey 08801; and ‡Max-Planck-Institut für Kohlenforschung, Kaiser-Willhelm-Platz 1, D 45470 Mülheim an der Ruhr, Germany

We report on studies of the structure of bimetallic $Pd_{0.5}Cu_{0.5}$ clusters, using X-ray diffraction and computer simulations. The latter combine a lattice-type bond order metal simulation model with non-self-consistent electron density functional MD/MC-CEM calculations to predict the geometry and the microstructure of clusters. Simulations at low and high temperatures were used to describe clusters with small and large amounts of positional (versus compositional) disorder. The structures obtained in the simulations exhibit face-dependent surface segregation, and layer-alternating concentration rich in one of the metal particles. For the disordered cluster, the simulation model predicts X-ray diffraction peaks and relative peak intensities in good agreement with the experiment.   © 1997 Academic Press

I. INTRODUCTION

The study of the chemical and physical properties of highly dispersed transition metals and alloys at the nanometer scale is of fundamental and practical interest. Mature technologies such as heterogeneous catalysis and photography rest on the special properties of small metal particles, and the recent focus on nanoscale inorganic materials has raised the prospect of further applications derived from the structural and chemical properties of highly dispersed metals and their compounds. Detailed knowledge of the structure and composition of the very small ("nanosized") particles and a quantitative understanding of the influence of high surface area on the macroscopic properties are key to an investigation of these materials.

The extensive application of highly dispersed metals in heterogeneous catalysis has resulted in their intensive examination in the form of supported metal crystallites. Such particles comprise both the free metal surface and the portion of the surface in contact with the support. Here we are interested in investigating small metal particles in the form of polymer-stabilized nanoscale metal colloids. Metals can be prepared as colloidal suspensions by well-controlled chemical methods, resulting in a narrow particle size distribution provided the medium is chemically isotropic and interacts only weakly with the metal surface. Since nanoparticles have 10–80% of their atoms on the surface, they present ideal systems for studying surface-related effects and probing small metal particle chemistry (1).

These considerations are particularly important in the case of highly dispersed alloys. The alloying of one metal with another is known to have a profound effect on the catalytic chemistry of metal surfaces (2). Bimetallic catalysts containing Pt and Ir or Re have found extensive use in the catalytic reforming of petrochemicals, while other prototype bimetallic systems have been investigated from a fundamental perspective. The chemical and physical properties of bimetallic surfaces are not always simply related to the bulk composition of the material. In fact, the preferential segregation of one component from the bulk to the surface is common (3). Factors influencing this phenomenon are complex, and are further obscured by the effect of adsorbates which may bind preferentially to one component of the alloy, thus changing the overall surface equilibrium. In the case of nanoscale alloys, these segregation effects can perturb the concentration profile several atomic layers into the bulk. For example, in a particle with a diameter of 2 nm, the vast majority of its 400–500 atoms is within a few atomic layers of the surface, and is thus susceptible to the influence of surface segregation.

Attention has focused on alloys of Gp 10 metals with Gp 11 metals, since the alloying of the catalytically active (Gp 10) metal with the less active (or inactive) Gp 11 metal can dramatically modify the surface chemistry of the metal (4). Prepared as highly dispersed colloids, stabilized by organic polymers, alloys of Pd and Cu are amenable to structural and spectroscopic analysis (5–9). The structure and surface properties of these colloidal alloys have been studied, in the context of both catalytic reactions and surface segregation phenomena, by infrared spectroscopy of adsorbed CO (5, 6), and by EXAFS analyses (10).

In this paper we describe results of X-ray diffraction measurements on polyvinylpyrrolidone-stabilized PdCu alloys,

complemented by a theoretical study in which the structure of a hypothetical 1289-atom $Pd_{0.5}Cu_{0.5}$ cluster is computed using the bond order metal simulation (BOS) model and the corrected effect medium (CEM) theory. For this structure, we explicitly compare theoretical and experimental X-ray diffraction patterns.

The paper is organized as follows. In Section II, the samples and X-ray diffraction measurements are described. Theoretical models and simulation procedures are outlined in Section III, followed by results and discussion in Section IV and a summary in Section V.

II. EXPERIMENTAL

Palladium–copper particles with nominal composition Pd_xCu_{1-x} stabilized with polyvinylpyrrolidone (PVP) were prepared in colloidal suspension from palladium acetate (0.45 mmol) and the appropriate amount of copper acetate monohydrate (MCB) by reduction in warm (90°C) 2-ethoxyethanol (35 ml) for 2 h under nitrogen. The temperature of the solution was kept below the boiling point of the solvent, to avoid occasional precipitation of solids. Concentrations of the metal salts were adjusted appropriately in the preparation of sols with the composition $Pd_{0.5}Cu_{0.5}$. Particle sizes of the resulting colloidal alloys were determined by small-angle X-ray scattering and transmission electron microscopy (TEM) to be ca. 60 and 100 Å (11).

The powder X-ray diffraction measurements were performed on Exxon beamline x01B at the National Synchrotron Light Source, Brookhaven National Laboratory. The beamline employs a vertically bent flat mirror and a horizontally bent Si(111) crystal to produce a focused X-ray beam at the sample. X-ray photons of 13, 108 eV (0.946 Å) were used in these powder measurements.

The X-ray powder diffraction patterns of Pd clusters were obtained by subtraction of the PVP scattering from the total scattering intensity. Since the PVP only gives slowly varying diffusion intensity near the Pd−Cu diffraction peaks, the intensity subtraction is rather straightforward. The observed diffraction patterns are discussed below.

The powder X-ray diffraction intensity, I_{eu}, in electron units can be calculated easily for clusters by the familiar Debye equation (12),

$$I_{eu} = \sum_m \sum_n f_m f_n \frac{\sin(q r_{mn})}{q r_{mn}}, \qquad [1]$$

where $q = 4\pi \sin\theta/\lambda$, 2θ is the angle between incident and scattered rays, λ is the wavelength of the X rays, $\bar{r}_{mn} = \bar{r}_m - \bar{r}_n$, with $\bar{r}_m$ the position vector of atom m, and f_m is the scattering factor of atom m. Application of Eq. [1] requires knowledge of the atomic positions in the cluster. For small clusters, one often uses a trial and error approach (13) guided by the equilibrium phase diagram, if known.

The Cu−Pd phase diagram has been studied extensively (14). Near the compositions of $Pd_{0.5}Cu_{0.5}$, the low-temperature bulk alloy is an ordered superstructure on a bcc lattice. We were unsuccessful in generating the experimental pattern of $Pd_{0.5}Cu_{0.5}$ cluster on the base of the known crystalline phases (15). We therefore turned to an atomic-scale simulation to obtain the atomic positions of the cluster.

III. THEORETICAL MODELS AND SIMULATION PROCEDURE

We use the lattice-type BOS model (16, 17) to determine the bulk-surface segregation and the surface microstructure of $Pd_{0.5}Cu_{0.5}$ clusters at 300 K. In the BOS model, the interaction energy for a binary system of N atoms, {A_i, $i = 1, \ldots, N$}, of two types ("A" or "B") is expressed as a sum of the site energies,

$$\Delta E(\{A_i\}) = \sum_{i=1}^{N} \varepsilon_{Z_i, M_i \text{ of } \beta_i}^{\alpha_i}, \qquad [2]$$

where α_i and β_i are either A-type or B-type atoms, N is the total number of atoms in the system, and Z_i and M_i are the coordination number (i.e., number of nearest neighbors) and number of unlike atoms around the central atom of type α_i, respectively. The site energy for an A-type atom surrounded by M atoms of type B and Z-M atoms of type A is written as

$$\varepsilon_{Z, M \text{ of } B}^{A} = \varepsilon_Z^A + M\Delta E_{Z, A-B}^A + \frac{M(M-1)}{2}\lambda_{Z,A-B}^A, \qquad [3]$$

where ε_Z^A is the interaction energy for a Z-coordinated A-type atom with all A-type neighbors, $\Delta E_{Z,A-B}^A$ is the energy change of the first A−B bond compared to an A−A bond, and $\lambda_{Z,A-B}^A$ is the incremental variation due to additional A−B bonds. The expression for $\varepsilon_{Z,M \text{ of } A}^B$ is obtained from Eq. [3] by simply interchanging As with Bs.

All six BOS parameters, ε_Z^A, ε_Z^B, $\Delta E_{Z, A-B}^A$, $\Delta E_{Z, B-A}^B$, $\lambda_{Z, A-B}^A$, and $\lambda_{Z, B-A}^B$, are determined from the experimental dimer bond energies, surface energies, cohesive energies, and bulk mixing energies as a function of composition (17, 18). The values of ε_Z^{Pd} (in eV) are -2.07, -2.38, -2.69, -3.00, and -3.89 for $Z = 6$, 7, 8, 9, and 12, respectively. The corresponding values for ε_Z^{Cu} (in eV) are -2.11, -2.33, -2.55, -2.77, and -3.49. To determine the four mixing parameters, $\Delta E_{12, Pd-Cu}^{Pd}$, $\Delta E_{12, Pd-Cu}^{Cu}$, $\lambda_{12, Pd-Cu}^{Pd}$, and $\lambda_{12, Pd-Cu}^{Cu}$, the ordered structure is used due to the large negative bulk mixing energies for the PdCu system. The resulting values (in kJ/mol) are -1.09, -4.31, 0.34, and 0.41, reproducing perfectly the experimental bulk mixing energies (in kJ/mol) of -1.18, -7.89, -10.70, -8.93, and -1.31, at the composition of $Cu_{1/32}Pd_{31/32}$, $Cu_{1/4}Pd_{3/4}$, $Cu_{1/2}Pd_{1/2}$,

and $Cu_{31/32}Pd_{1/32}$, respectively (19). Parametrization using the disordered structure does not change the structural results in this paper significantly because the most important information is the mixing energy for the $Cu_{1/2}Pd_{1/2}$ system.

Since the BOS model does not take the atomic size mismatch into account, we have used the non-self-consistent electron density functional CEM theory (20, 21) to do so. The simplest molecular-dynamics/Monte Carlo (MD/MC)-CEM form (21, 22) was used to model the geometry of the $Pd_{0.5}Cu_{0.5}$ clusters at different temperatures in order to introduce positional disorder. Note that the BOS model provides the geometrical mixing disorder on a lattice. In this MD/MC-CEM theory, the interaction energy of a system containing N atoms, relative to the state in which all atoms are infinitely far apart, is given by

$$\Delta E(\{A_i\}) = \sum_{i=1}^{N} \Delta F_{EXLM}(A_i; n_i) + \frac{1}{2} \sum_{i=1}^{N} \sum_{j \neq i}^{N} V_c(i, j), \quad [4]$$

where the "jellium" electron density surrounding atom A_i is

$$n_i = \frac{1}{2} \sum_{j \neq i}^{N} \int \frac{n(A_i; \mathbf{r} - \mathbf{R}_i)}{Z_i} n(A_j; \mathbf{r} - \mathbf{R}_j) d\mathbf{r}. \quad [5]$$

Here, $n(A_i; \mathbf{r} - \mathbf{R}_i)$ is the atomic electron density at $\mathbf{r}$ for atom A_i, with atomic number Z_i and nuclear position $\mathbf{R}_i$, and is obtained from Hartree–Fock calculations. $\Delta F_{EXLM}(A_i; n_i)$ is the "effective" embedding function for atom A_i, determined by forcing Eq. [5] to duplicate the cohesive energy curve of the bulk and the homonuclear diatomic binding curve (23). $V_c(i, j)$ is the Coulomb interaction between atom A_i and A_j, including nuclear–nuclear, nuclear–electron, and electron–electron terms, and is dependent only upon the already specified atomic electron density. The details of the MD/MC-CEM theory can be found in the original papers (20–23).

In summary, the lattice-type BOS model does not include the atomic size effect, although it is quite accurate in the prediction of the bulk-surface segregation and the surface microstructure (16, 17). By contrast, the MD/MC-CEM theory includes the influence of atomic size but is less accurate in the predication of the surface energies and the heats of mixing as compared with the BOS model (24). In this study, we use successive simulations, combining the BOS model with the MD/MC-CEM theory, to predict the geometry and the microstructures of $Pd_{0.5}Cu_{0.5}$ clusters, including both atomic arrangements and distances.

We first applied the BOS model to study the microstructure of the $Pd_{0.5}Cu_{0.5}$ clusters, at 300 K, using a perfect cubo-octahedral shaped 1289-atom cluster which is obtained from the ideal fcc lattice structure. This cluster has 482 surface atoms (or a 37% dispersion) of which 24, 108, 54, and 296 atoms occupy the corner, edge, fcc(100), and

fcc(111) sites, respectively; 5×10^7 MC steps were utilized to determine the equilibrium structures at this temperature, and convergence of results was validated by repeated calculations with different initial atomic assignments and MC random numbers.

The geometries of the $Pd_{0.5}Cu_{0.5}$ clusters at different temperatures are obtained by MD simulations with the MD/MC-CEM theory. Specifically, the structure of the low-temperature 1289-atom $Pd_{0.5}Cu_{0.5}$ cluster is obtained through a quench, starting from the cubo-octahedral shaped structure obtained from the BOS simulation at 300 K. During the quench (in a $3N$-dimensional coordinate space, where N is the number of active atoms), all atoms in the cluster can move according to their force fields, and any exchanges in atomic positions are prohibited. At the end of the quench, the maximum force on each atom is less than 1×10^{-5} eV/Bohr. The resulting cluster becomes more compact than the lattice structure, due to the relaxation caused from the size mismatch, but it retains the microstructure arrived at in the BOS simulation. From now on this structure is referred to as the ordered cluster.

In order to introduce more disorder into the $Pd_{0.5}Cu_{0.5}$ cluster, we thermalized the above ordered cluster at a high temperature (2000 K) for a short time (1 ps). During this anneal, every atom in the cluster can move continuously, but the relative positions of atoms do not change because of the short time of the simulation. The choice of anneal temperature and anneal time aims at reproducing the experimental X-ray diffraction pattern, while maintaining the microstructure from the BOS simulation (see also below). We do not believe that the experimental data are for a cluster at 2000 K, of course. This is just a convenient theoretical method for introducing a considerable amount of positional disorder into the $Pd_{0.5}Cu_{0.5}$ cluster. From now on this structure is referred to as the disordered cluster.

IV. RESULTS AND DISCUSSION

The structures of 1289-atom $Pd_{0.5}Cu_{0.5}$ ordered and disordered clusters are shown in Fig. 1. Note that the ordered cluster has sharp fcc(111) and fcc(100) faces, while the disordered cluster exhibits large distortions which are nevertheless within the atomic arrangement set by the ordered cluster. In other words, the general arrangement of atoms is the same in the ordered and disordered clusters, but the former exhibits a lattice-like structure while the latter exhibits considerable atomic positional variation around the lattice sites.

In the clusters of Fig. 1, Cu atoms preferentially occupy corner, edge, and fcc(100) surface sites, while Cu and Pd atoms mix well on the remaining fcc(111) sites. Overall, the first layer of the cluster is enriched with Cu atoms, while the second layer is Pd-rich. There are two key factors driving this particular surface segregation pattern and the
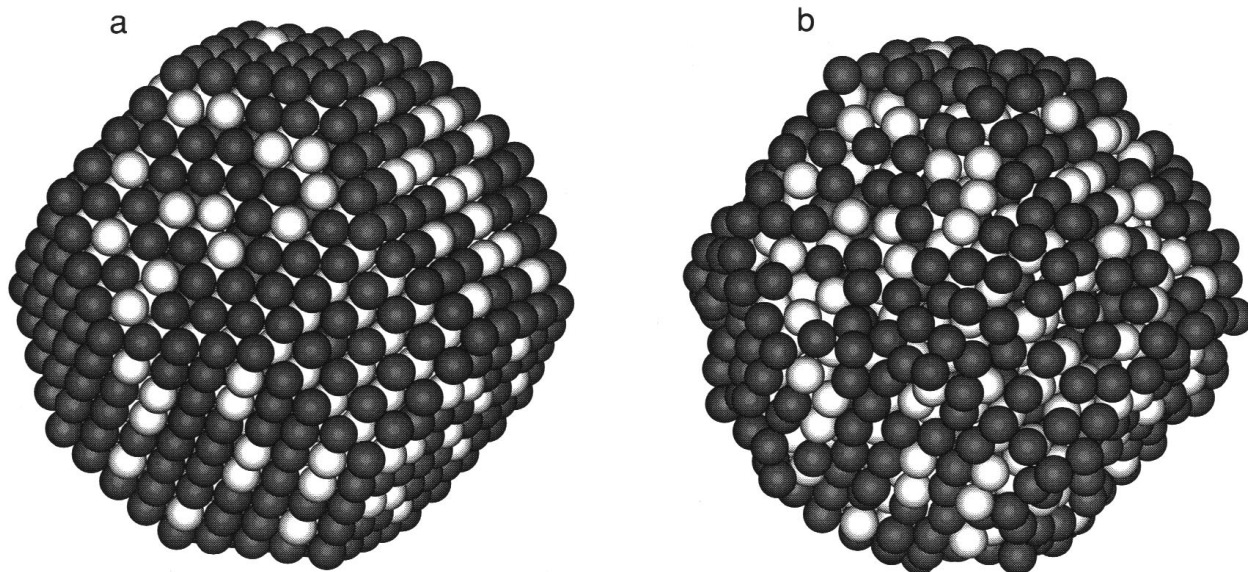
a
b

FIG. 1. The structures of 1289-atom $Pd_{0.5}Cu_{0.5}$ clusters predicted by the theoretical model. Cu atoms are dark spheres. (a) The ordered alloy obtained at low temperature; (b) the disordered alloy obtained at high temperature.

detailed variation of atomic concentration with layer: (i) the smaller surface energy of Cu relative to Pd forces the former to preferentially populate the surface vs bulk; and (ii) the negative mixing energy forces Pd to preferentially populate the first subsurface layer and to mix with Cu on the (111) facets.

The face-dependent surface segregation and the layer-alternating atomic concentration in the $Pd_{0.5}Cu_{0.5}$ cluster, obtained from the BOS simulation, have been observed for other systems in previous experimental and theoretical studies (25–27). At present, there are no experimental investigations on single crystals of PdCu for comparison, although an "average" over different faces is consistent with the limited experimental information that is available. What we will compare in this paper is the interior cluster structure from experiment and theory, as discussed in the following paragraphs.

The theoretical X-ray diffraction patterns, calculated from Eq. [1] for the above two clusters, are shown in Fig. 2. The disordered cluster has much smaller relative peak intensities, especially for large momentum transfer, reflecting a reduction in long-range order, relative to the ordered cluster. The small shift to the left in the peak positions for the disordered cluster is due to thermal expansion.

The PVP-background-corrected experimental X-ray diffraction patterns are shown in Fig. 3 for 60 and 100 Å $Pd_{0.5}Cu_{0.5}$ clusters. Note that these patterns exhibit peaks at all positions predicted by our theoretical study. However, the relative intensities of these peaks are very different from those obtained in the model with the ordered cluster. For example, in the experimental spectra of Fig. 3, the (220) reflection (i.e., the second peak) is shown only as very weak

peaks for the 60 and 100 Å clusters. A detailed comparison in Fig. 3 indeed shows that the theoretically predicted X-ray diffraction pattern for the disordered cluster matches closely the experimental measurement for the 60 Å cluster.

We do need to point out some discrepancies observed between theoretical and experimental patterns shown in Fig. 3. The experimental patterns exhibit additional diffuse tail at the high-q side of the second peak. This suggests that the experimentally formed clusters contain defects which are not explainable by simple thermal disorder. We also notice that the 100 Å cluster has peak width similar to that
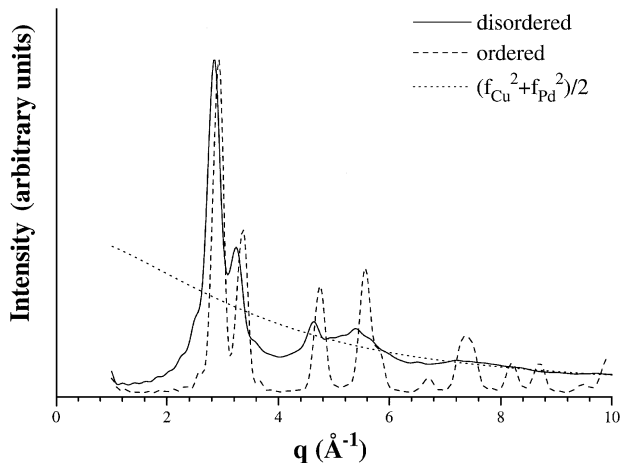

FIG. 2. The X-ray diffraction patterns calculated for the two clusters of Fig. 1. Note the oscillation of the X-ray diffraction intensities around the average scattering factor, $(f_{Cu}^2 + f_{Pd}^2)/2$.
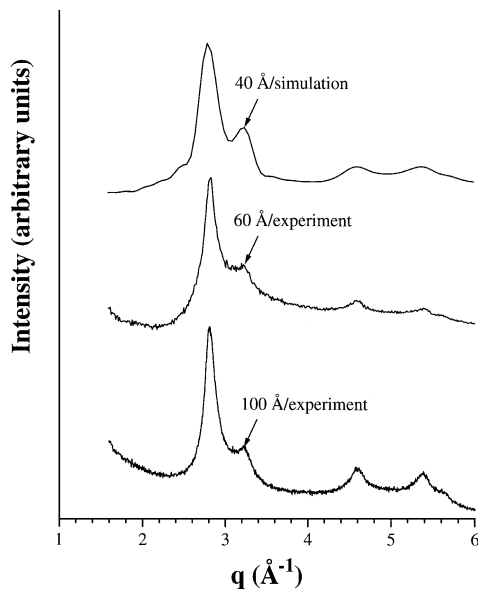
FIG. 3. Experimental X-ray diffraction patterns for $Pd_{0.5}Cu_{0.5}$ clusters of 60 and 100 Å in diameter, as compared to the model calculation for the disordered $Pd_{0.5}Cu_{0.5}$ cluster of 40 Å in diameter.

of the 60 Å cluster. This is attributed to the presence of twin in the larger clusters, as seen in the STM.

V. SUMMARY

We investigated the structures of bimetallic Pd–Cu clusters with both X-ray diffraction technique and theoretical simulations. We find that the combination of the lattice-type BOS model and the MD/MC-CEM theory can predict the geometry and microstructure of real clusters, thereby providing valuable insight into microstructure-controlling parameters.

Our main result is that the microstructure of $Pd_{0.5}Cu_{0.5}$ clusters exhibits face-dependent surface segregation, and layer-alternating atomic concentration profiles. Further experimental measurements will be crucial in verifying these predictions. We have also found that the thermal positionally disordered $Pd_{0.5}Cu_{0.5}$ cluster has an X-ray diffraction pattern which agrees reasonably well with the experimental cluster except for an apparent discrepancy in the cluster size and a diffuse tail in diffusion pattern. We suggest that the experimental Pd–Cu cluster has an other defect in addition to thermal disorder.

REFERENCES

1. Bradley, J. S., *in* "Clusters and Colloids" (G. Schmid, Ed.), pp. 459–544. VCH, Weinheim/New York, 1993.
2. Sinfelt, J. H., "Bimetallic Catalysts: Discoveries, Concepts and Applications." Wiley, New York, 1983.
3. Dowben, P. A., and Miller, A., (Eds.), "Surface Segregation Phenomena." CRC Press, Boca Raton, 1990.
4. Mallt, T., Szab, S., and Petr, J., *Appl. Surf. Sci.* **40**, 309 (1990).
5. Bradley, J. S., Hill, E. W., Chaudret, B., and Duteil, A., *Langmuir* **11**, 693 (1995).
6. Bradley, J. S., Hill, E. W., Klein, C., Chaudret, B., and Duteil, A., *Chem. Mater.* **5**, 254 (1993).
7. Toshima, N., and Wang, Y., *Chem. Lett.* **1993**, 1611 (1993).
8. Toshima, N., and Wang, Y., *Langmuir* **10**, 4574 (1994).
9. Toshima, N., and Wang, Y., *Adv. Mater.* **6**, 245 (1994).
10. Bradley, J. S., Via, G., Bonneviot, L., Hill, E., and Klein, C., submitted for publication.
11. Liang, K. S., and Bradley, J. S., unpublished data.
12. Warren, B. E., "X-Ray Diffraction." Addison-Wesley, Reading, MA, 1964.
13. Liang, K. S., Chien, F. Z., Hughes, G. J., Meitzner, G. D., and Sinfelt, J. H., *J. Phys. Chem.* **95**, 9974 (1991).
14. Subramanian, P. R., and Laughlin, D. E., *J. Phase Equilibria* **12**, 231 (1990).
15. Zhang, B., and Liang, K. S., unpublished data.
16. Zhu, L., and DePristo, A. E., *J. Chem. Phys.* **102**, 5342 (1995).
17. Zhu, L., and DePristo, A. E., *J. Catal.* **167**, 400 (1997).
18. Yang, L., and DePristo, A. E., *J. Catal.* **148**, 575 (1994).
19. Hultgren, R., Desai, P. D., Hawkins, D. T., Gleiser, M., and Kelley, K., "Selected Values of the Thermodynamic Properties of Binary Alloys." Univ. Microfilms, Ann Arbor, MI, 1990.
20. (a) Kress, J. D., and DePristo, A. E., *J. Chem. Phys.* **87**, 4700 (1987). (b) *J. Chem. Phys.* **88**, 2596 (1988).
21. (a) Raeker, T. J., and DePristo, A. E., *Int. Rev. Phys. Chem.* **10**, 1 (1991). (b) DePristo, A. E., *in* "Recent Advances in Density Functional Theory," Vol. 1, Part 1, Chap. 6, "Methodology" (D. Chong, Ed.). World-Scientific, Singapore, 1996.
22. Stave, M. S., Sanders, D. E., Raeker, T. J., and DePristo, A. E., *J. Chem. Phys.* **93**, 4413 (1990).
23. Kelchner, C. L., Halstead, D. M., Perkins, L. S., Wallace, N. M., and DePristo, A. E., *Surf. Sci.* **310**, 425 (1994).
24. (a) Raeker, T. J., and DePristo, A. E., *Phys. Rev. B* **49**, 8663 (1994). (b) Sinnott, S. B., Stave, M. S., Raeker, T. J., and DePristo, A. E., *Phys. Rev. B* **44**, 8927 (1991).
25. Mecke, K. R., and Dietrich, S., *Phys. Rev. B* **52**, 2107 (1995).
26. Reichert, H., and Dosch, H., *Surf. Sci.* **345**, 27 (1996).
27. Florencio, J., Ren, D. M., and Tsong, T. T., *Surf. Sci.* **345**, L29 (1996).